Escola de Primavera de Transição e Turbulência
Blumenau 2022

ABCM
13th Spring School on Transition and Turbulence
September 19th-23rd, 2022, Blumenau, SC, Brazil

EPTT-2022-0045
LINEAR STABILITY ANALYSIS OF THE BOUNDARY LAYER FLOW PAST GAPS IN BYPASS TRANSITION CONDITIONS

Victor Barcelos Victorino
Marcello Augusto Faraco de Medeiros
SAA, EESC, USP, zip code 13566-590
barcelos.victorino@usp.br, marcello@sc.usp.br

Marlon Sproesser Mathias
Institute of Advanced Studies - USP, zip code 05508-060
marlonsmathias@gmail.com

Abstract. *Boundary layer turbulence transition provokes a significant impact on aerodynamic drag. The boundary layer transition is related to its stability, therefore, it is crucial to understand the phenomena to build models that accurately predict the transition location. Additionally, several surface imperfections occur in a real aircraft's boundary layer, among them the presence of gaps. Recent studies demonstrated that, depending on the gap geometry and flow conditions, the physics of the boundary layer's transition deviates from its usual form. Therefore, the main objective of the present study is to investigate the impact of gaps on the boundary layer stability. We chose as parametric space the threshold for the transition dominated by Tollmien-Schlichting waves and another bypass mechanism, according to the literature. We developed a numerical study via two-dimensional direct numerical simulation as a precursor stage to get a equilibrium solution (base flow) of the compressible Navier-Stokes Equations. Next, we analyzed the flow stability to two- and three-dimensional disturbances. We conducted the linear stability analysis through an in-house algorithm that uses an Arnoldi-based time-stepping method. The study revealed unstable oscillation modes for 2D (Rossiter) and 3D (centrifugal) analysis. The stability limits of centrifugal modes were lesser than the Rossiter's in the flow conditions covered. The runs immediately preceding the bypass transition presented a weakly unstable Rossiter mode, whereas runs that occurred bypass, according to Crouch, Kosorygin and Sutanto (2020), presented strong oscillations attributed to the Rossiter mode. The frequency agreed within 4% of relative error compared to the literature. The numerical results supported the conjecture that the centrifugal instability causes 3D flow over the gap and the Rossiter mode triggers the transition.*

Keywords: *boundary layer, instability, gap.*

1. INTRODUCTION

Many studies have focused on the boundary layer because it is extensively present in the aeronautical field. The shear forces in the boundary layer have dissipative nature as a characteristic. Specifically in an aircraft, these forces contribute to drag in the form of viscous skin friction. Drag implies penalizing part of the thrust produced by the engine. As a consequence, engineering has an economic interest in its reduction. In addition, aircraft certification entities impose increasingly challenging targets regarding the level of greenhouse gases emission. To illustrate the impact on economic and environmental aspects, Schneider (2001) quantifies that a hypothetical reduction of 1% in the total aerodynamic drag of a large commercial aircraft operating over long distances would result in savings of 400,000 liters of fuel and a decrease of 5,000 kg of noxious gases emitted per year. Also, Marec (2001) states that about 50% of the total drag of a typical civil transport aircraft resides in viscous drag.

A boundary layer commonly becomes turbulent through a transition process. Concisely, it typically involves the receptivity of the boundary layer to natural disturbances present in the flow, followed by an oscillatory motion that amplifies up to the turbulent breakdown. In two-dimensional boundary layers, the fundamental oscillation mode is called the Tollmien-Schlichting (T-S) wave, after Tollmien (1931) and Schlichting (1933), the first authors to stablish the linear stability theory. Such a mechanism was evidenced first by Schubauer and Skramstad (1948). Concerning the transition location detection, van Ingen (1956) and Smith and Gamberoni (1956) independently suggested a semi-empirical method based on the linear stability theory. The e^N method correlates the transition region to the locus where the T-S wave growth ratio reaches a certain threshold determined experimentally. Still, other dynamics may arise in the transition process, such as transient growth or bypass transition, according to Saric *et al.* (2002).

Many authors investigate the impact of surface imperfections on the T-S growth and, hence, on the transition form and location. Perraud *et al.* (2014), through a numerical model, compared the factor N variation (ΔN) computed by the T-S growth in a boundary layer with the presence and the absence of a gap. The authors noted that ΔN was independent of the cavity depth for cavities with aspect ratio $L/D < 3.33$. Also, they broke down the variation into a localized effect

that affects the growth, exclusively near the gap, ΔN_{peak}, and a shift in the curve for positions far downstream from the cavity, ΔN_{far}. Forte *et al.* (2015) performed an experimental investigation to validate the model proposed by Perraud *et al.* (2014). The authors evidenced a critical condition where the transition occurs practically over the gap. The cavity length was a relevant parameter for such. Beguet *et al.* (2017) gathered results from several experimental, numerical, and theoretical researches on this topic. The study revealed the limits for the critical conditions according to the gap length and depth normalized by the displacement thickness, $L/\delta^* \geq 18$ and $D/\delta^* \geq 2$, respectively. Crouch and Kosorygin (2020) performed experimental correlations, investigating step, regular protrusion, and gap effects on the boundary layer transition. The linear combination of the ΔN correlation from the forward-facing and backward-facing step modeled well the results for the rectangular protrusion. However, the model was best represented only by a backward-facing step correlation for shallow gaps. Crouch *et al.* (2020) also experimentally performed ΔN correlations for cavity influence on transition with different aspect ratios and sizes. They observed that in a particular run with geometry corresponding to the critical condition, the oscillation frequency was about five times greater than the frequency content expected for the most magnified T-S for this flow condition, characterizing bypass transition.

Earlier investigations exhibited instabilities related to the presence of a cavity immersed in the boundary layer flow. Krishnamurty (1955) observed acoustic radiation in the flow over cavities through the schlieren technique and hot-wire anemometry. Plumblee *et al.* (1962) developed a theoretical model for cavity characteristic resonant response. Later, Rossiter (1964) proposed a physical mechanism to explain the acoustic radiation marked by a distinct tonal frequency experienced in particular flow conditions and cavity geometry. Rossiter also developed a semi-empirical correlation to estimate the frequency. According to him, separation occurs as the boundary layer passes through the cavity leading edge, forming a shear layer over the cavity mouth. Vortices (similar to Kelvin-Helmholtz eddies) occur inside the shear layer and collide with the trailing edge as it convect downstream. The impingement generates acoustic waves that travel back to the leading edge, destabilizing the shear layer and completing the feedback cycle. East (1966) experimentally confirmed the semi-empirical correlation by Rossiter (1964). Block (1976) also developed an analytical expression to predict the cavity resonant frequency with good agreement with experimental results. A few years later, Sarohia (1977) conducted an extensive series of experiments to investigate the role of the cavity shear layer on pressure oscillation and also determine the threshold of the onset of flow oscillation. The results from distinct flow conditions and cavity geometry collapsed into a single curve through a non-dimensional parameter, $(L/\delta)\sqrt{Re_\delta}$. Cattafesta *et al.* (1998) accomplished experiments to understand whether multiple Rossiter modes coexist or switch back and forth. According to them, when the flow conditions favor more than one Rossiter mode, the dominant mode alternatively switches among them. Yamouni *et al.* (2013) performed a global stability analysis of the open cavity flow. Their results suggested that the Rossiter mechanism predominates in low Mach. They also observed an overshoot in the amplification of unstable Rossiter modes when coupled with the acoustic modes from Plumblee *et al.* (1962). Likewise, Mathias and de Medeiros (2018) also observed this coupling between Rossiter and acoustic resonance. The authors further performed a parametric sweep to study the Rossiter dependency on the Mach number and the displacement thickness over the gap. They concluded that the incoming boundary layer plays a role in selecting which Rossiter mode will occur, whereas the Mach increases the acoustic energy transfer and, consequently, the temporal growth of the mode. Sun *et al.* (2017) investigated the stability of compressible flows over open cavities. In the subsonic regime, $M_\infty < 0.6$, an increment in Mach raised the instability. However, in the transonic regime, the Rossiter mode stabilized as the Mach was increased, mainly for the cavity with a larger aspect ratio.

Furthermore, the cavity flow presents an instability with three-dimensional nature, the centrifugal mode. Bayly (1988) performed an analytical approach to extend Rayleigh's centrifugal instability theory for inviscid two-dimensional flows. According to the study, the instability condition happens when closed convex streamlines have a decreasing circulation in the outward direction. Albensoeder *et al.* (2001) numerically investigated modes for finite and infinite lid-driven cavity flow. For shallow cavities, the most unstable fluctuations were a pair of oscillatory modes with a short wavelength. The amplitude function presented relevant intensity near the downstream edge of the gap. Depending on flow conditions and the geometry, two distinct modes occurred for aspect ratio close to the unit: a stationary or a pair of oscillatory modes. Faure *et al.* (2007) performed a series of flow visualization experiments to comprehend the 2-D and 3-D topology of the flow past open cavities. They reported the presence of three-dimensional structures for a range of Reynolds numbers and aspect ratios. Brés and Colonius (2008) numerically investigated the stability of three-dimensional perturbations in two-dimensional compressible subsonic flows over open cavities. Their results indicated the presence of three unstable modes (modes I, II, and III), differing from each other in the frequency range, including a stationary mode (mode I). According to them, this instability arose due to a non-acoustic nature, attributed to a mechanism of centrifugal instability. They also found a low dependence of the centrifugal mode in the Mach number, while the Reynolds number exerted influence on the instability level and the hierarchy of the dominant mode. De Vicente *et al.* (2014) numerically and experimentally investigated the centrifugal instability in flow regimes where the Rossiter mode was absent. The authors constructed the neutral diagram for different spanwise wavenumbers and Reynolds and reported a rich experimental characterization of the flow's oscillation structures. The study by Meseguer-Garrido *et al.* (2014) numerically scanned an extensive parametric space to survey the neutral and amplification curves of the centrifugal mode. The authors noted the presence of two three-

dimensional modes, a bifurcated one with oscillatory and stationary components, depending on the flow conditions, and a purely traveling mode. Sun *et al.* (2017) compared the linear stability analysis with 3D DNS results. The authors advised that cavities with larger aspect ratios had relevant non-linear interactions between the 2D and 3D modes, diverging from the linear assumptions of stability analysis. Mathias and de Medeiros (2020) numerically investigated the interaction between Rossiter and centrifugal modes. The authors noted that in the 3D DNS, the spectrum peaks associated with the Rossiter were less sharp than in the 2D runs. They attributed this to a spanwise modulation of the Rossiter due to the centrifugal modes. According to them, such motion could alter the base flow, consequently its stability.

This paper addresses the linear stability analysis of the two-dimensional flow past a gap located over a flat plate. We chose the parameter space (Reynolds, Mach, gap geometry, etc.) based on the conditions where bypass transition occurred, according to Crouch *et al.* (2020). In a particular run where turbulence transition took place over the gap, Crouch *et al.* (2020) measured a frequency substantially higher than a frequency content expected from a T-S wave in such conditions. Therefore, the objective is to investigate unstable modes present in the previously mentioned problem and to correlate the actual outcomes with the experimental results from the literature.

2. METHODOLOGY

The present section describes the numerical approach, consisting of two stages: the direct numerical simulation (DNS) and the linear stability analysis. The DNS approximates an unsteady solution of the Navier-Stokes Equations without turbulence modeling. The long-term solution will reach a steady-state if the flow is globally stable. The equilibrium solution is necessary once it is the base flow for the modal analysis. In contrast, in the case of a globally unstable flow, it is possible to dampen the oscillations through the selective frequency damping (SFD) technique to reach the base flow, as proposed by Åkervik *et al.* (2006). The linear stability analysis assesses the stability, neutrality, or instability from a base flow to two- or three-dimensional disturbances. To attain the oscillation modes from the base flow, we used the algorithm implemented by Mathias (2017), which evaluates the eigenvalues and eigenfunctions of the flow Jacobian matrix, which in turn is approximated by an Arnoldi-based time-stepping method.

2.1 Direct Numeric Simulation

The DNS solver is an in-house code developed by this research group. Details of the implementation of the code are provided in the current section, albeit a supplementary reading is available in Bergamo (2014), Martinez (2016), Mathias (2017), and Mathias (2021). To enhance the computational efficiency, the solver runs in Fortran 90 language, and the 2DECOMP&FFT library performs the processing parallelization. The scientific computational software Matlab employs pre and post-processing. The compressible Navier-Stokes Equations (NSE) are used to model the flow. As acoustic resonance within the gap can cause the Rossiter instability, the solver must assess compressibility effects. Here, we present the equations used by the numeric solver:

$$\frac{\partial \rho}{\partial t} = -\rho \frac{\partial u_i}{\partial x_i} - u_i \frac{\partial \rho}{\partial x_i}, \tag{1}$$

$$\frac{\partial u_j}{\partial t} = -u_i \frac{\partial u_j}{\partial x_i} - \frac{1}{\rho}\frac{\partial p}{\partial x_j} + \frac{1}{\rho}\frac{\partial \tau_{ij}}{\partial x_i}, \tag{2}$$

$$\frac{\partial e}{\partial t} = u_i \frac{\partial e}{\partial x_i} - \frac{p}{\rho}\frac{\partial u_i}{\partial x_i} + \frac{\tau_{ij}}{\rho}\frac{\partial u_j}{\partial x_i} - \frac{1}{\rho}\frac{\partial q_i}{\partial x_i}, \tag{3}$$

where the viscous stress tensor and heat flux are given by

$$\tau_{ij} = \frac{\mu}{Re}\left(\frac{\partial u_i}{\partial x_j} + \frac{\partial u_j}{\partial x_i} - \frac{2}{3}\delta_{ij}\frac{\partial u_k}{\partial x_k}\right), \tag{4}$$

$$q_i = -\frac{\mu}{(\gamma - 1)\, Re\, Pr\, M_\infty^2}\frac{\partial T}{\partial x_i}, \tag{5}$$

respectively. The flow variables are density, ρ, and the three velocity componenents, $\vec{V} = u\hat{i} + v\hat{j} + w\hat{k}$. State equations for ideal gas supplement the NSE for the pressure, p. The viscosity is obtained through Sutherland's Law. The Navier Stokes Equations, equations 1, 2, and 3, refer to the equations obtained by deriving the physical laws of conservation of mass, momentum, and energy in a fluid, respectively. All flow variables are non-dimensional, normalized by their appropriate scales.

The DNS code uses a structured Cartesian mesh for domain discretization, with a standard uniform spacing. However, one can employ grid refinement in particular regions where are expected higher derivative values. The domain presents buffer zones at the open boundaries to avoid the reflection of oscillations, thus providing suitable far-field conditions.

Two factors inherent to buffer zones contribute to this: (i) the spacing between the nodes gradually increases towards the boundaries and (ii) the reduced accuracy order of the method used for spatial derivatives computing. A smooth transition between the spatial derivative methods occurs due to the linear combination of both methods. Figure 1 exhibits the typical mesh spacing for the current DNS. The yellow dashed line indicates the stream-wise position of the gap leading edge, whereas the purple dashed line indicates the gap trailing edge.

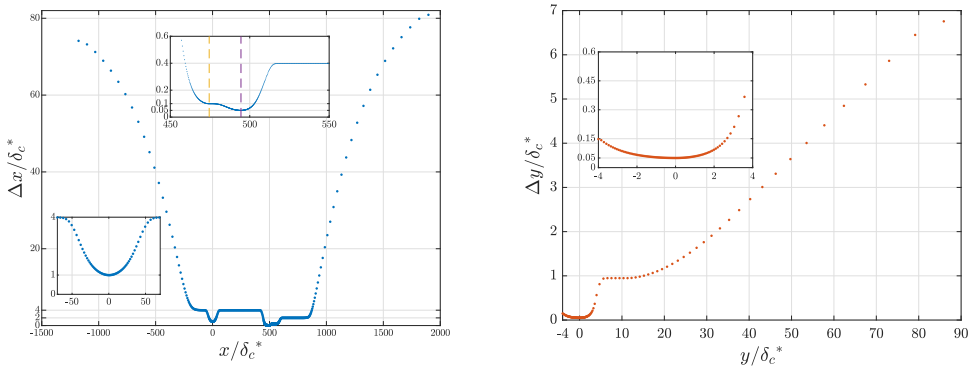

(a) Stream-wise axis x. (b) Wall-normal axis y.

Figure 1: Mesh spacing as a function of the coordinate axis.

To approximate spatial derivative terms, a compact finite differences scheme is used, with spectral-like resolution according to the method proposed by Lele (1992). On the upstream boundary condition, we use a uniform flow with constant energy and null stream-wise pressure gradient. At the outlet, boundary conditions are a null second-derivative with a prescribed pressure. Similarly occurs in the outflow boundary, where all variables have null second-derivatives. At the bottom boundary, the incident flow is modeled as a free-slip wall with null cross-flow derivative $\partial U/\partial y$, whereas the flat plate has isothermal condition for the energy, no-slip and no-penetration for velocity, and a null pressure-gradient in the normal direction. A 10th order low-pass anti-aliasing filter, proposed by Gaitonde and Visbal (1998), aids to dissipate the motion in wavelengths shorter than the mesh resolution. The method employed for time marching is the fourth-order Runge-Kutta method. The initial condition is the Blasius numerical solution.

2.2 Instability Analysis

According to Juniper *et al.* (2014), the modal approach is the fundamental mathematical tool for analysis of the flow instability subject to small-amplitude perturbations. However, complex flows like the actual open cavity problem do not allow the assumption of parallel flow. Ergo, the Orr-Sommerfeld Equation is not suitable. Consequently, the global instability analysis is the proposed method to evaluate the flow's eigenspectrum, as Theofilis (2011). There are two distinct manners to calculate the flow's eigenspectrum: the matrix-forming or the time-stepping method. For the present flow, the latter is advantageous once do not requires the cumbersome task of computing an expensive matrix. Hence, we employed the method implemented by Mathias (2017), based on Tezuka and Suzuki (2006). The Jacobian matrix, which contains the oscillating modes of the base flow, is numerically approximated by Arnoldi's method, according to Arnoldi (1951). Arnoldi's algorithm is opportune to evaluate the unstable modes present in the flow because it converges readily for the less damped modes. The real part of the flow's eigenvalues, $\Re\{\sigma\}$, is associated with the growth rate, whereas the imaginary part, $\Im\{\sigma\}$, indicates the circular frequency of the mode. For each eigenvalue, there is an associated eigenfunction, ϕ, which corresponds to the spatial shape of the mode.

3. RESULTS

Here we present the results. Firstly, we show the base flow from both aspect ratios covered ($L/D = 5$ and 10) , followed by the outcome from the two and three-dimensional stability analysis. Table 1 displays the runs covered and their respective parameters. The geometric parameter L is the length of the gap in the stream-wise axis and D is the gap's depth. There are also flow parameters: δ^*, which states for the boundary layer displacement thickness over the gap's leading edge, M_∞, that indicates the free-stream Mach number, and the Reynolds number, Re, based on different length scales. We sought to reproduce two different aspect ratios because the possible unstable modes are highly dependent on the geometry. However, more focus was given to the aspect ratio $L/D = 5$, once Crouch *et al.* (2020) measured a particular frequency out of the unstable range for the T-S mode. Such oscillation led to the bypass transition, according to them.

Table 1: Flow parameters for the present study.

Run	L/δ^*	D/δ^*	L/D	Re_{δ^*}	Re_D	Re_L	M_∞
L17D3	17.50	3.50	5.00	1312	4591	22956	0.053
L20D4	20.00	4.00	5.00	1405	5621	28106	0.065
L24D2	24.00	2.40	10.00	1470	3528	35280	0.065
L26D2	26.00	2.60	10.00	1297	3372	33715	0.053
L27D2	27.50	2.75	10.00	1370	3764	37640	0.060

3.1 Base flow

The instability analysis requires a very tight accuracy. Because the method runs the DNS to filter the less stable modes, persistent small oscillation in the flow can contaminate the actual flow's modes or cause the emergence of spurious modes. Consequently, one advises time variations of about the order of magnitude of the machine epsilon to consider a proper steady solution. In the present study, the maximum absolute iteration residuals for the flow's variables had values of about 10^{-13}.

Figure 2 exhibits streamlines and vorticity of the base flow from the runs L20D4 and L27D2. It is possible to observe the presence of accentuated vorticity near the gap trailing edge in both geometries. In Fig. 2a, a primary vortex occurs with a diameter of approximately one-quarter of the gap's length. A pair of elongated counter-rotating secondary eddies occupy the remaining gap's space. For the shallower cavity, we notice the presence of an extra pair of vortices, as shown in Fig. 2b. Close to the downstream end, an eddy with a diameter close to the gap's depth also occurs. However, the superior secondary vortex appears to be two vortices merged. The central vortex has a size slightly smaller than the primary vortex. Near the bottom of the gap, two weak counter-rotating vortices appear in the interstices of the three superior vortices.

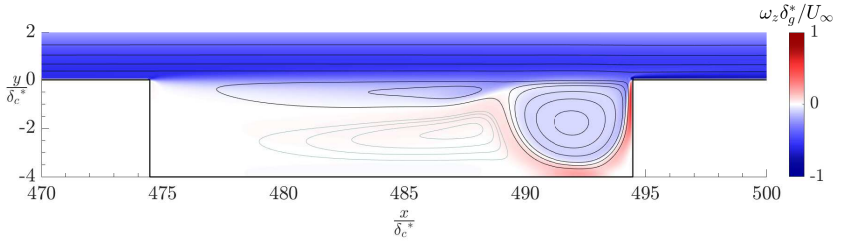

(a) run L20D4

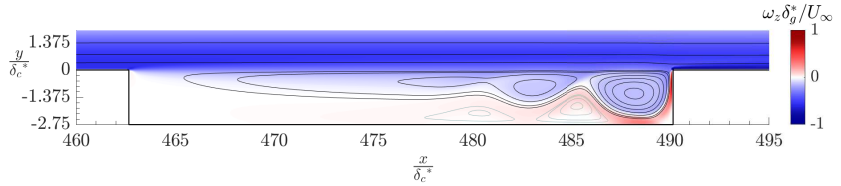

(b) run L27D2

Figure 2: Iso-contours of the non-dimensional spanwise vorticity and stream-lines of the base flow.

3.2 Rossiter instability

Firstly, we performed the two-dimensional instability analysis to verify the presence of the Rossiter mode, in other words, a mode with a null spanwise wavenumber, $\beta = 0$, or an infinite spanwise wavelength, $\lambda_z = \infty$. Figure 3 displays the flow's eigenvalues spectrum for both gap's aspect ratio, $L/D = 5$ in Fig. 3a and $L/D = 10$ in Fig. 3b. The run L17D3 presented a marginally unstable state with a small amplification factor. Moreover, the run L20D4 exhibited an amplification rate one order of magnitude greater. The imaginary part of the eigenvalues gives us the circular frequency of the mode. It is possible to observe that the frequency tends to decrease as increasing the gap length, as the expression given by Rossiter (1964). A similar behavior happened with the second aspect ratio. The runs that anticipated the transition location by altering the T-S growth, according to Crouch *et al.* (2020), presented a stable Rossiter mode in L24D2 and a marginally unstable one in L26D2. Again, the critical run displayed a Rossiter mode with a considerably greater amplification rate. The difference between the two aspect ratios was the hierarchy of the dominant Rossiter mode. For $L/D = 5$, the Rossiter second mode (R_2) was dominant, whereas the Rossiter third mode (R_3) prevailed for $L/D = 10$.

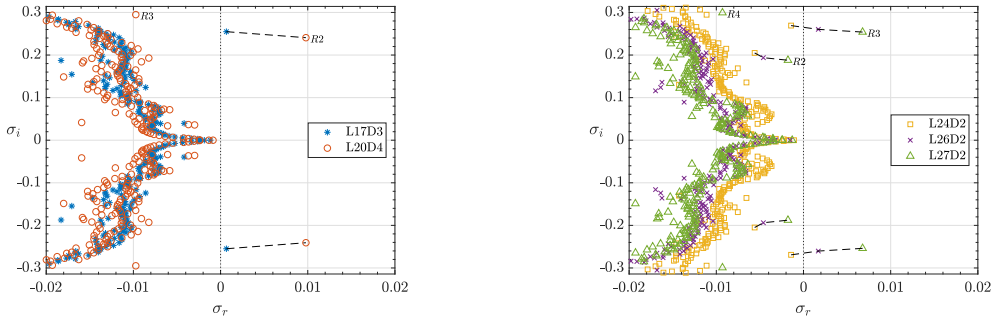

(a) $L/D = 5$ (b) $L/D = 10$

Figure 3: Eigenvalues spectra from the runs with aspect ratio $L/D = 5$ (a) and $L/D = 10$ (b) in the complex plane. The imaginary axis indicates the circular frequency, whereas the real corresponds to amplification or damping rate.

Another aspect that occurred for the aspect ratio $L/D = 10$ was the presence of the second Rossiter mode moving towards instability. A slightly wider gap or the same geometry with a greater Reynolds or Mach number possibly would present multiple unstable Rossiter modes simultaneously. Finally, we noticed that the range from the dominant Rossiter mode frequency does not vary, even with a drastic change in the aspect ratio, remaining around 0.25 rad/s. The frequency of the run L20D4 agreed within 4% of relative deviation in comparison with the frequency experimentally measured by Crouch *et al.* (2020) in the similar run, namely the *Case C*.

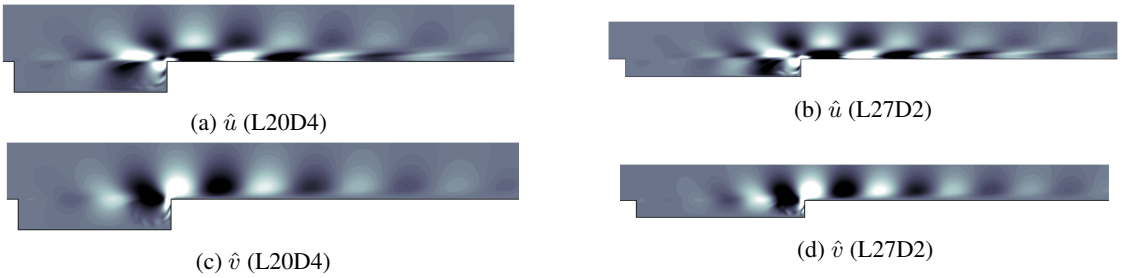

(a) $\hat{u}$ (L20D4) (b) $\hat{u}$ (L27D2)

(c) $\hat{v}$ (L20D4) (d) $\hat{v}$ (L27D2)

Figure 4: Eigenfunctions of the the most unstable Rossiter mode, R_2, from the run L20D4 in (a) and (c), and R_3 from L27D2 in (b) and (d).

Figure 4 reveals the iso-contours of the eigenfunctions from the flow variables $\hat{u}$ and $\hat{v}$ from the runs L20D4 and L27D2, in an arbitrary phase. The eigenfunctions were quite similar to Rossiter shape modes reported in the literature, for instance Rowley (2002), Theofilis and Colonius (2004), Sun *et al.* (2017), and Mathias and de Medeiros (2018). In Fig. 4a and Fig. 4c, we can see the presence of two vortices inside the gap, leading to the conclusion that such oscillation mode was the Rossiter second mode (R_2). In opposite, in Fig. 4b and Fig. 4d, it can be seen three vortices that occupy the gap. The mode shape reveals that the oscillatory flow, caused by the gap instability, extends to the boundary layer up to far downstream. A curious fact concerning the streamwise velocity eigenfunctions, $\hat{u}$, is that the spatial amplitude distribution downstream of the gap presents a phase shift of π, at $y/\delta_g^* \approx 1$, between the inner and the outer peaks, similarly to the T-S mode shape.

3.3 Centrifugal instability

We performed the three-dimensional linear stability analysis to investigate the presence of the centrifugal mode. The solver assumes periodicity in the spanwise axis when called by the time-stepping method. We must specify a spanwise wavenumber as input for that. The cumbersome task is to perform a parametric sweep for several spanwise wavelengths, $\lambda_z = 2\pi/\beta$. The procedure was to find the lower instability limit and gradually change the λ_z/D parameter up to the upper limit. Figure 5 presents the complex eigenvalue spectra for the unstable range of spanwise wavelengths. The spanwise wavelength range with unstable modes was $0.25 \leq \lambda_z/D \leq 2.8$ for the aspect ratio $L/D = 5$, and $0.25 \leq \lambda_z/D \leq 9.75$ for $L/D = 10$. The most unstable mode for $L/D = 5$ had a spanwise wavelength $\lambda_z/D = 0.5$, while $\lambda_z/D = 1.0$ for $L/D = 10$. In the runs L17D3, L26D2, and L27D2, the dominant three-dimensional eigenvalue was an oscillatory mode, whereas, in the run L20D4, the most unstable was a standing mode.

It is possible to observe unstable modes of several kinds, including the three modes identified by Brés and Colonius (2008). Figure 6 displays the streamwise velocity eigenfunction, from the aspect ratio $L/D = 5$, in a phase where its real projection maximum matches the absolute maximum. Furthermore, the figure exhibits the streamlines from the base flow,

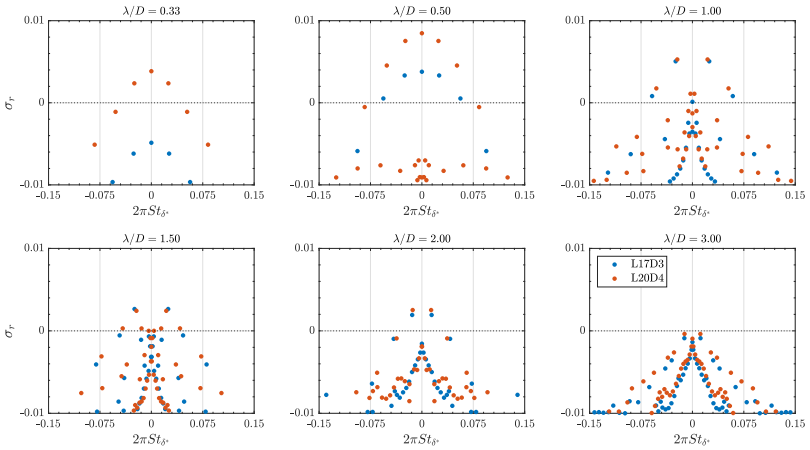

(a) $L/D = 5$

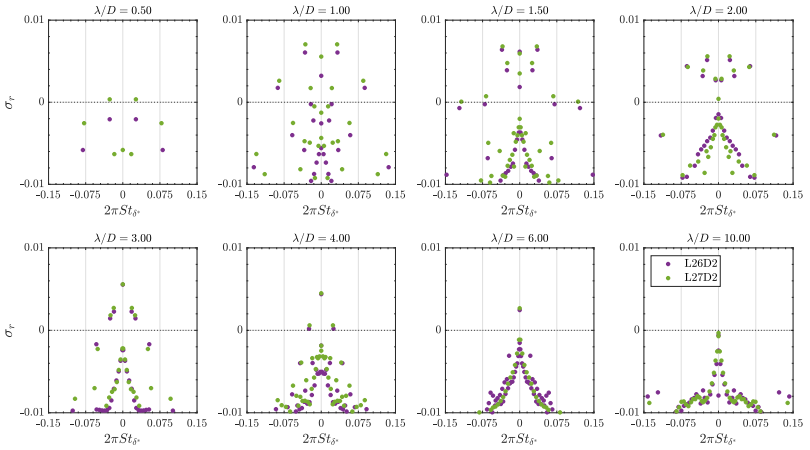

(b) $L/D = 10$

Figure 5: Spectra of eigenvalues for the centrifugal modes with several spanwise wavenumbers for L/D=5 in (a) and $L/D = 10$ in (b).

with clockwise streamlines represented by solid lines. The analysis shows that the shape of the stationary mode, *mode I*, resembles the traveling mode eigenfunction of *mode II*. According to Brés and Colonius (2008), *mode II* is the mode with the largest strouhal number. Both aforementioned modes show a great parcel of the oscillatory motion around the primary vortex, located downstream of the gap. Alternatively, *mode III*, also a traveling mode, had spatial structures more intense near the upstream region of the cavity. Also, one can note an abrupt decrease in its temporal frequency compared to *mode II*.

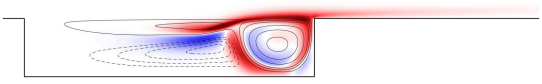

(a) Mode I (stationary)

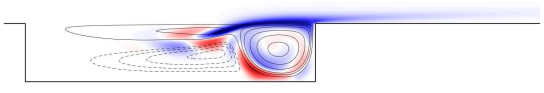

(b) Mode II (traveling)

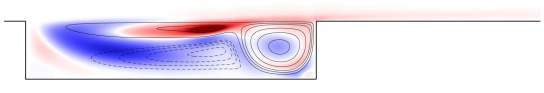

(c) Mode III (traveling)

Figure 6: Stream-wise velocity eigenfunctions, $\hat{u}$, of centrifugal modes from run L20D4.

3.4 Discussion

The two-dimensional linear stability analysis revealed the presence of the Rossiter mode in the parametric space close to the bypass transition threshold in the diagram from Crouch *et al.* (2020). For both aspect ratios, we have found a Rossiter mode with a low amplification rate in the flow condition that anticipates the critical condition, according to Crouch *et al.* (2020), while a strong amplification rate occurred in the run corresponding to the bypass transition. Furthermore, this correlation was stronger for $L/D = 5$. The circular temporal frequency of the different Rossiter modes remained close to 0.25 rad/s. The Rossiter frequency from the run L20D4 agreed within 4% compared to the experimentally measured by Crouch *et al.* (2020) in the correspondent run where bypass transition occurs. Such frequency is about two times the frequency of branch II of the T-S unstable frequency range for the Reynolds number around $Re_{\delta*} = 1400$. Therefore, a coupling between Rossiter and T-S is unlikely in such flow conditions. The linear stability results suggest that the Rossiter mode plays a role in turbulence transition.

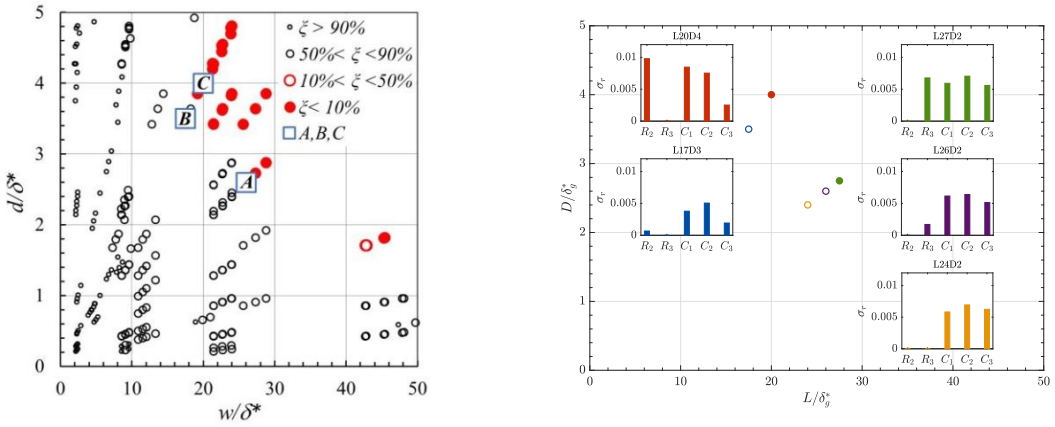

(a) Crouch *et al.* (2020).

(b) Present study.

Figure 7: Correlation of the impact on the boundary layer transition as a function of the gap geometry, according to Crouch *et al.* (2020), and the modes from the linear stability analysis (bar plot). Open markers indicate transition by T-S waves, whereas filled markers, bypass transition.

These cases also presented several three-dimensional centrifugal modes within a range of spanwise wavenumbers, including the presence of stationary and traveling centrifugal modes. The results indicated that the centrifugal instability limits were lesser than the neutrality for the Rossiter mode. Furthermore, the stability analysis revealed centrifugal modes with a temporal frequency close to the T-S unstable range of frequencies for the local Reynolds number. The centrifugal instability could interact with the T-S wave, altering its growth (ΔN) in cases where the gap caused the transition to move upstream. Figure 7 summarizes the results and compares them with the experimentally obtained by Crouch *et al.* (2020). One can see a stronger correlation concerning the Rossiter instability rather than the centrifugal with the bypass threshold limits.

4. CONCLUSION

The present study addresses the numerical investigation via direct numerical simulation and linear stability analysis of the Blasius boundary layer with a gap with its reference length of the order of magnitude of the boundary layer thickness. The literature supported the choice of the flow conditions employed in the simulations. The parametric region aimed at gaps with the aspect ratio (L/D) of 5 and 10. The characterization of the base flows exhibited the presence of vortices inside the cavity, which were crucial to instability. For both aspect ratios, a primary vortex occurred in the downstream portion of the gap, whereas a secondary elongated vortex occupied the upstream region. The main difference from the aspect ratio of 5 to 10 was an extra vortex between the primary and secondary vortex. Later, we performed the linear stability analysis of the base flows. We also found that the dominant Rossiter mode changed from the aspect ratio of 5 to 10, from the Rossiter second mode (R_2) to the third mode (R_3).

The linear stability analysis supports that the centrifugal mode occurrence allows the flow to become three-dimensional, and the Rossiter mode triggers the transition. Other works from the literature reported the non-linear interaction between the Rossiter and Centrifugal modes, for instance, Sun *et al.* (2017), Mathias and de Medeiros (2020), and Mathias (2021). However, despite the presence of the Rossiter mode in the bypass transition condition, it is still unclear whether such mode causes the transition.

5. ACKNOWLEDGEMENTS

V.B.V. was sponsored by the National Council for Scientific and Technological Development (CNPq/Brazil), grant 134335/2018-0. M.S.M. was sponsored by São Paulo Research Foundation (FAPESP/Brazil), grant 2018/04584-0. M.A.F.M. thanks the CNPq/Brazil for grant 307956/2019-9, the US Air Force Office of Scientific Research (AFOSR) for grant FA9550-18-1-0112, managed by Dr. Geoff Andersen from SOARD, and FAPESP/Brazil for grant 2019/15366-7. The authors also thanks Jeffrey D. Crouch for kindly providing supporting data for the simulations.

6. REFERENCES

Åkervik, E., Brandt, L., Henningson, D.S., Hœpffner, J., Marxen, O. and Schlatter, P., 2006. "Steady solutions of the navier-stokes equations by selective frequency damping". *Physics of Fluids*, Vol. 18, No. 6, p. 068102. doi:10.1063/1.2211705.

Albensoeder, S., Kuhlmann, H.C. and Rath, H.J., 2001. "Three-dimensional centrifugal-flow instabilities in the lid-driven-cavity problem". *Physics of Fluids*, Vol. 13, No. 1, pp. 121–135. ISSN 10706631. doi:10.1063/1.1329908.

Arnoldi, W.E., 1951. "The principle of minimized iterations in the solution of the matrix eigenvalue problem". *Quarterly of Applied Mathematics*, Vol. 9, pp. 17–29.

Bayly, B.J., 1988. "Three-dimensional centrifugal-type instabilities in inviscid two-dimensional flows". *Physics of Fluids*, Vol. 31, No. 1, pp. 56–64. ISSN 0031-9171. doi:10.1063/1.867002.

Beguet, S., Perraud, J., Forte, M. and Brazier, J.P., 2017. "Modeling of transverse gaps effects on boundary-layer transition". *Journal of Aircraft*, Vol. 54, No. 2, pp. 794–801. ISSN 00218669. doi:10.2514/1.C033647.

Bergamo, L.F., 2014. *Instabilidade hidrodinâmica linear do escoamento compressível em uma cavidade*. Master's thesis, Escola de Engenharia de São Carlos. doi:10.11606/D.18.2014.tde-28052014-164324. URL `http://www.teses.usp.br/teses/disponiveis/18/18148/tde-28052014-164324/`.

Block, P.J.W., 1976. "Noise response of cavities of varying dimensions at subsonic speeds". Technical Note D-8351, National Aeronautics and Space Administration. URL `https://ntrs.nasa.gov/citations/19770007874`.

Brés, G.A. and Colonius, T., 2008. "Three-dimensional instabilities in compressible flow over open cavities". *Journal of Fluid Mechanics*, Vol. 599, pp. 309–339. ISSN 00221120. doi:10.1017/S0022112007009925.

Cattafesta, L.N., Garg, S.K. and Michael S. Jones, G.S., 1998. "Experiments on compressible flow-induced cavity oscillations". In *29th AIAA Fluid Dynamics Conference*. doi:10.2514/6.1998-2912.

Crouch, J.D. and Kosorygin, V.S., 2020. "Surface step effects on boundary-layer transition dominated by tollmien–schlichting instability". *AIAA Journal*, Vol. 58, No. 7, pp. 2943–2950. doi:10.2514/1.j058518.

Crouch, J.D., Kosorygin, V.S. and Sutanto, M.I., 2020. "Modeling Gap Effects on Transition Dominated by Tollmien-Schlichting Instability". *AIAA AVIATION Forum June 15-19*. doi:10.2514/6.2020-3075. URL `http://dx.doi.org/10.2514/6.2020-3075`.

De Vicente, J., Basley, J., Meseguer-Garrido, F., Soria, J. and Theofilis, V., 2014. "Three-dimensional instabilities over a rectangular open cavity: From linear stability analysis to experimentation". *Journal of Fluid Mechanics*, Vol. 748, pp. 189–220. ISSN 14697645. doi:10.1017/jfm.2014.126.

East, L.F., 1966. "Aerodynamically induced resonance in rectangular cavities". *Journal of Sound and Vibration*, Vol. 3, No. 3, pp. 277–287. ISSN 10958568. doi:10.1016/0022-460X(66)90096-4.

Faure, T.M., Adrianos, P., Lusseyran, F. and Pastur, L., 2007. "Visualizations of the flow inside an open cavity at medium range Reynolds numbers". *Experiments in Fluids*, Vol. 42, No. 2, pp. 169–184. ISSN 07234864. doi:10.1007/s00348-006-0188-8.

Forte, M., Perraud, J., Seraudie, A., Beguet, S. and Casalis, L.G.G., 2015. "Experimental and Numerical Study of the Effect of Gaps on Laminar Turbulent Transition of Incompressible Boundary Layers". *Procedia IUTAM*, Vol. 14, No. 0, pp. 448–458. ISSN 22109838. doi:10.1016/j.piutam.2015.03.073. URL `http://dx.doi.org/10.1016/j.piutam.2015.03.073`.

Gaitonde, D.V. and Visbal, M.R., 1998. "High-Order Schemes for Navier-Stokes Equations: Algorithm and Implementation Into FDL3DI". Technical Report 1998-3060, AIR FORCE RESEARCH LAB WRIGHT-PATTERSON. URL `https://apps.dtic.mil/sti/citations/ADA364301`.

Juniper, M.P., Hanifi, A. and Theofilis, V., 2014. "Modal stability theory". *Applied Mechanics Reviews*, Vol. 66, No. 2. ISSN 00036900. doi:10.1115/1.4026604.

Krishnamurty, K., 1955. "Acoustic radiation from two-dimensional rectangular cutouts in aerodynamic surfaces". Technical Note 3487, National Advisory Committee for Aeronautics, Washington, US. URL `https://digital.library.unt.edu/ark:/67531/metadc57843/`.

Lele, S.K., 1992. "Compact finite and difference schemes and with spectral-like and resolution". *Journal of Computational physics*, Vol. 103, pp. 16–42.

Marec, J.P., 2001. "Drag reduction: a major task for research". In *Aerodynamic Drag reduction technologies: proceedings of the CEAS, DragNet European Drag Reduction Conference 19 - 21 June 2000, Potsdam, Germany*. pp. 17 – 28. ISSN

0179-9614.

Martinez, A., 2016. *Towards natural transition in compressible boundary layers*. Ph.D. thesis, Escola de Engenharia de São Carlos.

Mathias, M.S., 2017. *Análise de instabilidade de escoamentos compressíveis sobre uma cavidade aberta por um método numérico sem formação de Jacobiano*. Master's thesis, Escola de Engenharia de São Carlos, Universidade de São Paulo.

Mathias, M.S., 2021. *Computational study of the hydrodynamic stability of gaps and cavities in a subsonic compressible boundary layer*. Ph.D. thesis, São Carlos School of Engineering, University of São Paulo.

Mathias, M.S. and de Medeiros, M.A.F., 2018. "The influence of the boundary layer thickness on the stability of the rossiter modes of a compressible rectangular cavity". *2018 Fluid Dynamics Conference*. doi:10.2514/6.2018-3386.

Mathias, M.S. and de Medeiros, M.A.F., 2020. "Interaction between rossiter and görtler modes in the compressible flow in an open cavity". *Aiaa Aviation 2020 Forum*, Vol. 1 PartF, pp. 1–6. doi:10.2514/6.2020-3074.

Meseguer-Garrido, F., De Vicente, J., Valero, E. and Theofilis, V., 2014. "On linear instability mechanisms in incompressible open cavity flow". *Journal of Fluid Mechanics*, Vol. 752, pp. 219–236. ISSN 14697645. doi:10.1017/jfm.2014.253.

Perraud, J., Arnal, D. and Kuehn, W., 2014. "Laminar-turbulent transition prediction in the presence of surface imperfections". *International Journal of Engineering Systems Modelling and Simulation*, Vol. 6, No. 3-4, pp. 162–170. ISSN 17559766. doi:10.1504/IJESMS.2014.063129.

Plumblee, H.E., Gibson, J.S. and Lassiter, L.W., 1962. "Theoretical and Experimental Investigation of The Acoustic Response of Cavities In An Aerodynamic Flow". *Technical Report*, , No. USAF Report WADD-TR-61-75, pp. 1–167.

Rossiter, J.E., 1964. "Wind-tunnel experiments on the flow over rectangular cavities at subsonic and transonic speeds". *Reports and Memoranda No. 3438 - Aeronautical Research Council - Ministry of Aviation*.

Rowley, C.W., 2002. *Modeling, Simulation, and Control of Cavity Flow Oscillations*. Ph.d., California Institute of Technology. doi:10.7907/G4ZX-KH73.

Saric, W.S., Reed, H.L. and Kerschen, E.J., 2002. "Boundary-layer receptivity to freestream disturbances". *Annual Review of Fluid Mechanics*, Vol. 34, No. 1, pp. 291–319. doi:10.1146/annurev.fluid.34.082701.161921. URL `https://doi.org/10.1146/annurev.fluid.34.082701.161921`.

Sarohia, V., 1977. "Experimental investigation of oscillations in flows over shallow cavities". *AIAA Journal*, Vol. 15, No. 7, pp. 984–991. ISSN 00011452. doi:10.2514/3.60739.

Schlichting, H., 1933. "Laminare strahlausbreitung". *ZAMM - Journal of Applied Mathematics and Mechanics / Zeitschrift für Angewandte Mathematik und Mechanik*, Vol. 13, No. 4, pp. 260–263. doi:10.1002/zamm.19330130403.

Schneider, W., 2001. "The importance of aerodynamics in the development of commercially successful transport aircraft". In *Aerodynamic Drag reduction technologies: proceedings of the CEAS, DragNet European Drag Reduction Conference 19 - 21 June 2000, Potsdam, Germany*. pp. 9–16.

Schubauer, G.B. and Skramstad, H.K., 1948. "Laminar boundary-layer oscillations and transition on a flat plate". *National Advisory Committee for Aeronautics - Report No. 909*.

Smith, A.M.O. and Gamberoni, N., 1956. "Transition, Pressure Gradient, and Stability Theory". Technical Report ES 26388, Douglas Aircraft Division.

Sun, Y., Taira, K., Cattafesta, L.N. and Ukeiley, L.S., 2017. "Biglobal instabilities of compressible open-cavity flows". *Journal of Fluid Mechanics*, Vol. 826, pp. 270–301. ISSN 14697645. doi:10.1017/jfm.2017.416.

Tezuka, A. and Suzuki, K., 2006. "Three-dimensional global linear stability analysis of flow around a spheroid". *AIAA Journal*, Vol. 44, No. 8, pp. 1697–1708. ISSN 00011452. doi:10.2514/1.16632.

Theofilis, V. and Colonius, T., 2004. "Three-dimensional instabilities of compressible flow over open cavities: Direct solution of the BiGlobal eivenvalue problem". *34th AIAA Fluid Dynamics Conference and Exhibit*, , No. June. doi:10.2514/6.2004-2544.

Theofilis, V., 2011. "Global linear instability". *Annual Review of Fluid Mechanics*, Vol. 43, No. 1, pp. 319–352. doi:10.1146/annurev-fluid-122109-160705. URL `https://doi.org/10.1146/annurev-fluid-122109-160705`.

Tollmien, W., 1931. "The production of turbulence". *National Advisory Committee for Aeronautics - Technical Memorandum no. 609*.

van Ingen, J.L., 1956. "A suggested semi-empirical method for calculation of the boundary layer transition region". *Technische Hogeschool Vliegtuigbouwkunde - Report V.T.H.-74*.

Yamouni, S., Sipp, D. and Jacquin, L., 2013. "Interaction between feedback aeroacoustic and acoustic resonance mechanisms in a cavity flow: A global stability analysis". *Journal of Fluid Mechanics*, Vol. 717, pp. 134–165. ISSN 00221120. doi:10.1017/jfm.2012.563.

7. RESPONSIBILITY NOTICE

The authors are the only responsible for the printed material included in this paper.